Journal of Power Sources 196 (2011) 1723–1729

Contents lists available at ScienceDirect

Journal of Power Sources

journal homepage: www.elsevier.com/locate/jpowsour

Mesoporous Pt and Pt/Ru alloy electrocatalysts for methanol oxidation

Esteban A. Franceschini[a], Gabriel A. Planes[b], Federico J. Williams[c], Galo J.A.A. Soler-Illia[d], Horacio R. Corti[a,c,*]

[a] Grupo de Celdas de Combustible, Departamento de Física de la Materia Condensada, Centro Atómico Constituyentes, CNEA. Av. General Paz 1499 (1650), San Martín, Buenos Aires, Argentina
[b] Departamento de Química, Facultad de Ciencias Exactas, Fisicoquímicas y Naturales, Universidad Nacional de Río Cuarto, Agencia Postal No 3, 5800, Río Cuarto, Argentina
[c] Departamento de Química Inorgánica, Analítica y Química-Física, INQUIMAE CONICET, Facultad Ciencias Exactas y Naturales, Pabellón 2, Ciudad Universitaria, Buenos Aires, Argentina
[d] Gerencia de Química, Centro Atómico Constituyentes, CNEA. Av. General Paz 1499 (1650), San Martín, Buenos Aires, Argentina

ARTICLE INFO

Article history:
Received 16 July 2010
Received in revised form 5 October 2010
Accepted 5 October 2010
Available online 13 October 2010

Keywords:
Methanol
Fuel cells
Mesoporous
PtRu alloys
Catalyst

ABSTRACT

Mesoporous Pt and Pt/Ru catalysts with 2D-hexagonal mesostructure were synthesized using a triblock poly(ethylene oxide)-b-poly(propylene oxide)-b-poly(ethylene oxide) copolymer (Pluronic F127®) template, on a gold support. Large electrochemical surface areas were observed for the catalysts prepared at high overpotentials. Compared to the Pt catalyst, the Pt/Ru alloy containing 3 at% of Ru exhibited lower onset potential and more than three times the limit mass activity for methanol oxidation. This behavior is assigned to the larger pore size of the mesoporous Pt and Pt/Ru catalysts obtained with this template that seems to improve the methanol accessibility to the active sites compared to those obtained using lyotropic liquid crystals.

1. Introduction

Metal deposits with a well defined periodic mesoporous nanostructure, usually supported over carbon particles, are receiving much attention as catalysts for the oxidation of methanol in direct methanol fuel cells (DMFC) [1–5]. Platinum and Pt/Ru alloys can be obtained by electrodeposition [5] or chemical reduction [6] of metallic precursors dissolved in the aqueous domains of the liquid crystalline phases of oligoethylene oxide surfactants, acting as mesostructural templates. These mesoporous structures exhibit a regular array of hexagonally packed pores [7] that combine high specific surface areas with a narrow distribution of open pores [8,9].

In the case of the templates formed by the nonionic surfactants octaethylene glycol monohexadecyl ether ($C_{16}EO_8$, Brij 56®) and decaethyleneoxide mono-octadecyl ether ($C_{18}EO_{10}$, Brij 76®), the obtained mesoporous metal deposits have high specific surface, due to the small pore size (2.5–3.4 nm in diameter) [6,7,10], but the hexagonal array, with pores almost parallel to the surface, and the small pore size would limit the methanol transport across the catalyst layer and diminish the effective electrochemical active area. It is expected that catalysts with larger pore diameter would enhance the methanol accessibility of methanol to the catalyst.

Hexagonal mesoporous materials with large pore size (~10 nm in diameter) can be obtained from copolymers with large polyethylene oxide (EO) segments, such as Pluronic F127® (triblock poly(ethylene oxide)-b-poly(propylene oxide)-b-poly(ethylene oxide) copolymer) if high concentrations of the copolymer are used in the electroplating mixture, even when the cubical phase is the most stable for aqueous F127® [11,12].

Ample evidence is available showing that the "cavity-crystals" obtained employing F127® as a template are larger in size than their analogues derived from low molecular weight surfactants, and have better thermal stability [13–16]. Moreover, its channel connectivity and pore size can be tuned by adjusting deposition parameters, such as the volume fraction of the polymer blocks, reaction temperature, and composition of the solution [14,15,17–19].

Mesoporous Pt/Ru alloys are recognized as a promising anode electrocatalysts in low-temperature polymer membrane fuel cells using methanol [6,20–22] and considerable efforts are devoted to obtain these mesoporous nanostructures in both, controlled and reproducible forms using mesostructural templates. Jiang and Kucernak [21] prepared unsupported mesoporous Pt/Ru catalysts by electrodeposition in Brij 56® and reported electrochemical

* Corresponding author at: Grupo de Celdas de Combustible, Departamento de Física de la Materia Condensada, Centro Atómico Constituyentes, CNEA. Av. General Paz 1499 (1650), San Martín, Buenos Aires, Argentina. Tel.: +54 11 6772 7174; fax: +54 11 6772 7121.
E-mail address: hrcorti@cnea.gov.ar (H.R. Corti).

0378-7753/$ – see front matter © 2010 Elsevier B.V. All rights reserved.
doi:10.1016/j.jpowsour.2010.10.016

active surface area (EAS) values of 78–81 $m^2 g^{-1}$, determined by CO and Cu stripping techniques, similar to the BET surface area value (86 $m^2 g^{-1}$) reported by Attard et al. [6] for the chemically prepared mesoporous Pt/Ru in Brij 76®. The EAS value for commercial (E-TEK) nanoparticulated Pt and Pt/Ru (1:1) catalysts supported on Vulcan XC-72 reported in the literature (measured by CO stripping) are 60 $m^2 g^{-1}$ and 43 $m^2 g^{-1}$ [23,24], respectively, although much higher values were also reported for the E-TEK Pt/Ru (1:1) catalysts [25].

In this work we prepare Pt and Pt/Ru catalysts with hexagonal mesostructure by electroreduction of the corresponding precursor salts dissolved in the aqueous domains of the Pluronic F127® block copolymer–water mesophase deposited on a gold substrate. The effect of the reduction potential upon deposition on the morphology and electrochemical efficiency for the methanol oxidation is analyzed.

2. Experimental

2.1. Chemicals

Triblock poly(ethylene oxide)-b-poly(propylene oxide)-b-poly(ethylene oxide) copolymer $EO_{106}PO_{70}EO_{106}$, denoted Pluronic F127® (Mw = 12,600, Aldrich), hydrated hexa-chloroplatinic acid (HCPA, 99.99%, Aldrich), ruthenium trichloride (99.99%, Aldrich), methanol (99.8%, Research S.A.) and sulfuric acid (PA grade, Research S.A.) were used as received. Solutions were prepared with deionized water (resistivity ≈18 MΩ cm), and degassed using high purity nitrogen. Commercial Pt/C catalyst (E-TEK, 20 wt.% Pt load), was used for control analysis.

2.2. Preparation of mesoporous catalysts

Metal precursor solutions were prepared by mixing 1 g of F127® with 1 cm^3 of 0.1 M HCPA for the platinum catalysts, and with 0.05 cm^3 of 0.2 M $RuCl_3$ and 0.95 cm^3 of 0.1 M HCPA for the Pt/Ru alloys, and mixing vigorously using a glass rod.

The viscous mixture was poured in a purpose-built three-electrode electrochemical cell having a gold working electrode (EMF company), a large surface area platinum counter electrode, and a Ag/AgCl(sat) reference electrode that was inserted in the mixture between the working and the counter electrode. The metals were reduced applying different potentials between −500 mV and −300 mV (vs. Ag/AgCl(sat) reference) during 30 min, in order to deposit alloys with different structures [7]. The Faradaic efficiency (FE) of the electrodeposition in the F127® template was obtained by weighting the mass of catalyst electrodeposited on the gold substrate employing a microbalance (Mettler XP2U). According to Lewera et al. [26], Pt in Pt/Ru alloys remains in metallic state, and the formation of oxides is not observed. On the other hand, the presence of ruthenium oxides is as much important as the metallic ruthenium but, in the FE calculation, the error of considering that Pt and Ru in the Pt(97)/Ru(3) deposited alloy are in metallic forms is negligible.

The chronoamperograms exhibit different behavior depending on the applied potential, as shown in Fig. 1. Nucleation and growth behavior are observed at overpotentials in the range from −400 to −450 mV [27]. The current increases observed in Fig. 1 around 100–150 s is characteristic of a growing step, as a consequence of the restriction in the diffusion of the catalysts precursors that originate the formation of a large number of embryos from which the structure will growth increasing its area [28–30]. The current peak decreases as the applied overpotential increases, and disappears completely at overpotentials of −300 mV for Pt and −400 mV for Pt/Ru alloys, as a consequence of the formation of smaller particles.

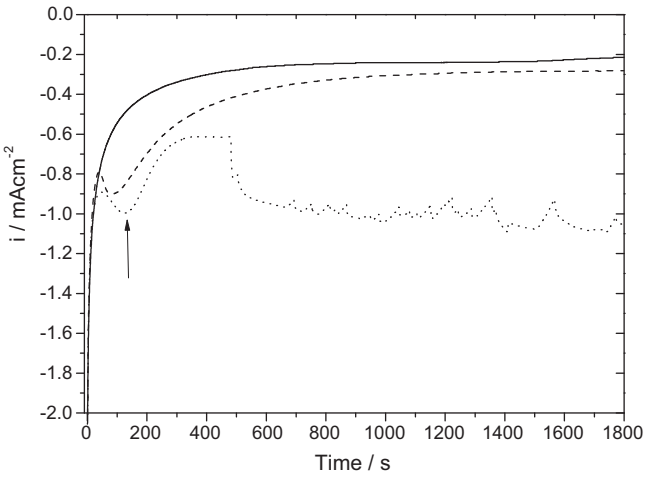

Fig. 1. Chronoamperometry of formation of Pt at −300 mV (continuous line), −400 mV (dashed line) and −500 mV (dotted line), and the grow peak is signed with an arrow.

Current fluctuations in the chronoamperograms are observed at very high overpotentials (higher than −450 mV for all cases), probably due to the reduction of water, generating gaseous products, such as H_2.

2.3. Electrochemical and morphological characterization

All electrochemical experiments were performed at 25 °C employing a potentiostat (TEQ_02, Argentina). After deposition, the electrodes were washed in deionized water by 24 h and cycled in 1 M H_2SO_4, between −205 mV and +645 mV vs. Ag/AgCl (sat) at a scan rate of 100 mV s^{-1} in order to remove surfactant residues from the surface and measure its electrochemical area. Methanol electro-oxidation experiments were performed in 0.5 M H_2SO_4/1.0 M methanol solutions purged with nitrogen. Chronoamperometric profiles were measured by applying a step potential from 45 to 445 mV vs. Ag/AgCl (sat) and recording the current transient for 2 h.

The STM images were acquired with a Veeco-DI Multimode Nanoscope IIIa, with 10 μm lateral scan range and a 2 μm z-scanner. The bias potential was fixed at 10 mV and the tunneling current at 1 nA, employing a Pt/Ir tip (Nano Devices, Veeco Metrology, Santa Barbara, CA).

Scanning electron micrographs were obtained using a Quanta 200 (FEI Company) SEM operating at a voltage of 25–30 kV, equipped with EDX. High resolution electron micrographs were obtained using a Supra 40 (Zeiss Company) FESEM operating at 3 kV.

X-ray Photoelectron Spectroscopy (XPS) measurements were performed under UHV conditions (base pressure < 5×10^{-10} mbar) in a SPECS UHV spectrometer system equipped with a 150 mm mean radius hemispherical electron energy analyzer and a nine channeltron detector. XPS spectra were acquired at a constant pass energy of 20 eV using an un-monochromated Mg Kα (1253.6 eV) source operated at 12.5 kV and 20 mA and a detection angle of 30° with respect to the sample normal on grounded conducting substrates. Quoted binding energies are referred to the adventitious C 1s emission at 285 eV. Atomic ratios and surface concentrations were calculated from the integrated intensities of core levels after instrumental and photoionization cross-section corrections.

Small Angle X-ray Scattering (SAXS) measurements of samples deposited on conductive substrates, prepared by sputtering of gold on thin microscope cover slides, were performed using the D11-A SAXS2 line of the National Synchrotron Light Laboratory (LNLS, Campinas, Brazil). The sample-detector distance was 807.2 mm,

λ = 1.488 Å, and the samples were observed in transmission mode at 3° with respect to the incident beam. The reported values of the cell dimensions are an average of at least three measurements, carried out on different regions of the sample, to ensure a correct characterization. Wide angle grazing-incidence X-ray diffraction (GI-XRD) scans were performed in the D10-A XRD2 line of LNLS, Campinas, Brazil at 8 keV energy. The sample-detector distance was 520 mm, λ = 1.5498 Å, and an incidence angle 0.8°, in order to sense only the sample metallic layer, and for 2θ values between 38° and 45°.

3. Results and discussion

3.1. Morphological analysis

Scanning electron micrographs at high scale were obtained to analyze whether the catalyst sample has a homogeneous granular structure, or exhibits fractures. In Fig. 2a–d different morphologies can be observed for the Pt (Fig. 2a and b) and the Pt/Ru (Fig. 2c and b) catalysts, at different electrodeposition overpotentials. For the catalysts deposited at low overpotentials (−300 mV vs. Ag/AgCl(sat) for Pt and −400 mV for Pt/Ru alloy), smooth structures formed by small particles were obtained (Fig. 2a and c). At higher overpotentials (<−450 mV vs. Ag/AgCl(sat)) granular structures, formed by larger particles than those obtained at low over-potentials were observed for both catalyst (Fig. 2b and d).

High-resolution electron micrographs of Pt and Pt/Ru confirm the mesoporous structure of the catalysts. As shown in Fig. 2e and f, for Pt and Pt/Ru, respectively, the catalyst layers are formed by porous spheres with a pore diameter of ∼10 nm (measured directly from the FESEM image). Both, the Pt catalyst and the Pt/Ru show the same mesoporous structure.

The EDX analysis reveals an atomic composition of 97% Pt and 3% Ru for the Pt/Ru alloy, without significant deviations on different regions of the sample.

The SAXS patterns obtained in transmission conditions at 3° incidence (Fig. 3) show well-defined diffraction spots, corresponding to highly ordered mesostructured metallic thin film coatings. Measurements carried out in normal incidence transmission mode show strong diffraction circles; these features demonstrate that samples are constituted by a mosaic structure (i.e., no *x*–*y* ordering) with domains presenting highly ordered mesopore planes parallel to the substrate [31]. The spot patterns present well-defined 2D-hexagonal (*p6m*) symmetry in all cases. Pt samples present a hexagonal cell parameter $a = 13.7 \pm 0.2$ nm. The cell presents a noticeable uniaxial pore contraction of 14% along the *z*-axis (Fig. 3a). In addition to the *p6m* pattern, two weak spots can be observed at $q_z = 0$, which are characteristic in-plane reflections of an *Im3m* cubic lattice [32,33]. The presence of these spots might be indicative of a mixture of hexagonal and cubic mesophases, or intermediate phases, which is due to their epitaxy relationship [34–36]. The presence of 3D-cubic-like domains can facilitate molecular mass transport because it would allow that an interconnection exists between the pores, which are mainly parallel, nevertheless this would not be an important effect in our catalysts.

Pt–Ru samples present a purely hexagonal mesostructure with $a = 11.6 \pm 0.1$ nm, and a slight distortion along the *z*-direction of 5%

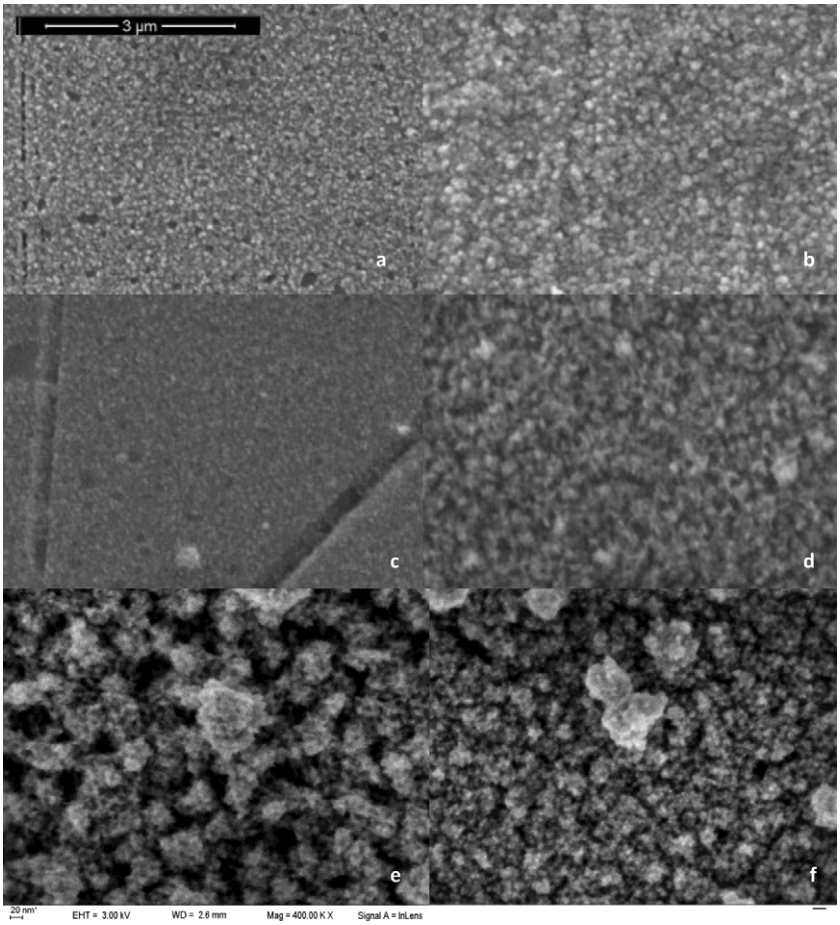

Fig. 2. SEM micrographs of Pt and Pt/Ru alloys obtained at different potentials. (a) Pt obtained at −300 mV; (b) Pt obtained at −400 mV; (c) Pt/Ru alloy obtained at −400 mV; (d) Pt/Ru alloy obtained at −425 mV. (e) High-resolution micrograph of Pt obtained at −400 mV. (f) High-resolution micrograph of Pt/Ru alloy obtained at −425 mV. The magnification of the micrographs a–d is 30,000×, while for e–f is 400,000×. All the potentials were measured vs. Ag/AgCl(sat) reference.

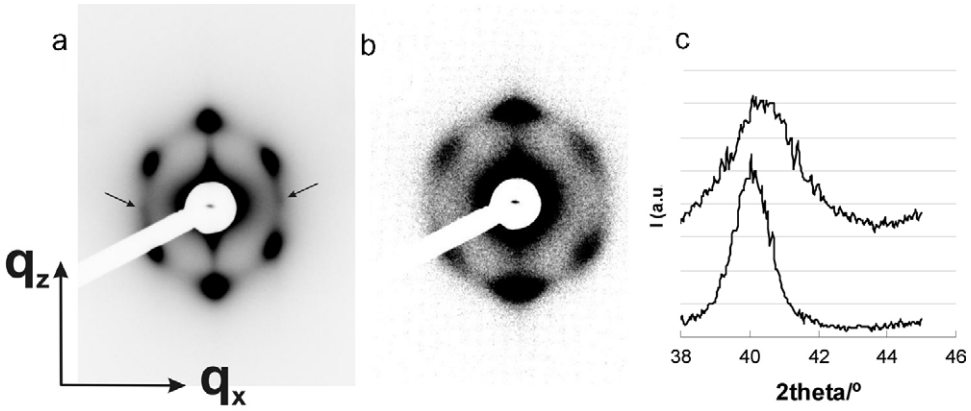

Fig. 3. SAXS patterns obtained in transmission at 3° of Pt (a) and Pt/Ru mesoporous thin films deposited onto a gold-covered thin glass substrate. Arrows in (a) indicate the weak signals corresponding to [1 1 0] in-plane reflections of an *Im3m* cubic mesophase. (c) Detail of the [1 1 1] peak region of the GI-XRD patterns of Pt (lower) and Pt–Ru (upper) samples.

(Fig. 3b). Although in both cases, a 2D hexagonal mesophase with cylindrical pores parallel to the surface is obtained, three factors can contribute to mass transport in the direction normal to the electrode:

(a) amphiphilic block-copolymer-templated materials present residual microporosity due to the strong interaction between the PEO block and the inorganic walls that enhances molecule transport [37],
(b) the mesopore channels are not mono-oriented, but present a mosaic-like texture; defects located in the boundaries between domains with different in-plane pore orientations permitting some accessibility to the electrode [38],
(c) the presence of some cubic-like domains (in the pure Pt sample).

Wide angle GI-XRD scans of both samples in the region of the [1 1 1] diffraction of Pt are shown in Fig. 3c. Large peaks are observed, characteristic of metallic nanoparticles that form the pore walls. The 2θ peak positions are 40.15° and 40.65° for the Pt and Pt(97)Ru(3) samples, leading to a cell parameter $a = 3.91$ Å and 3.86 Å, respectively.

An STM analysis was carried out in the order of elucidate the structure of the electrodeposits at low scale. In Fig. 4a it is observed that the catalyst structure is formed by a sphere array. The sectional view, at the left, indicates that the mean particle size is approxi-

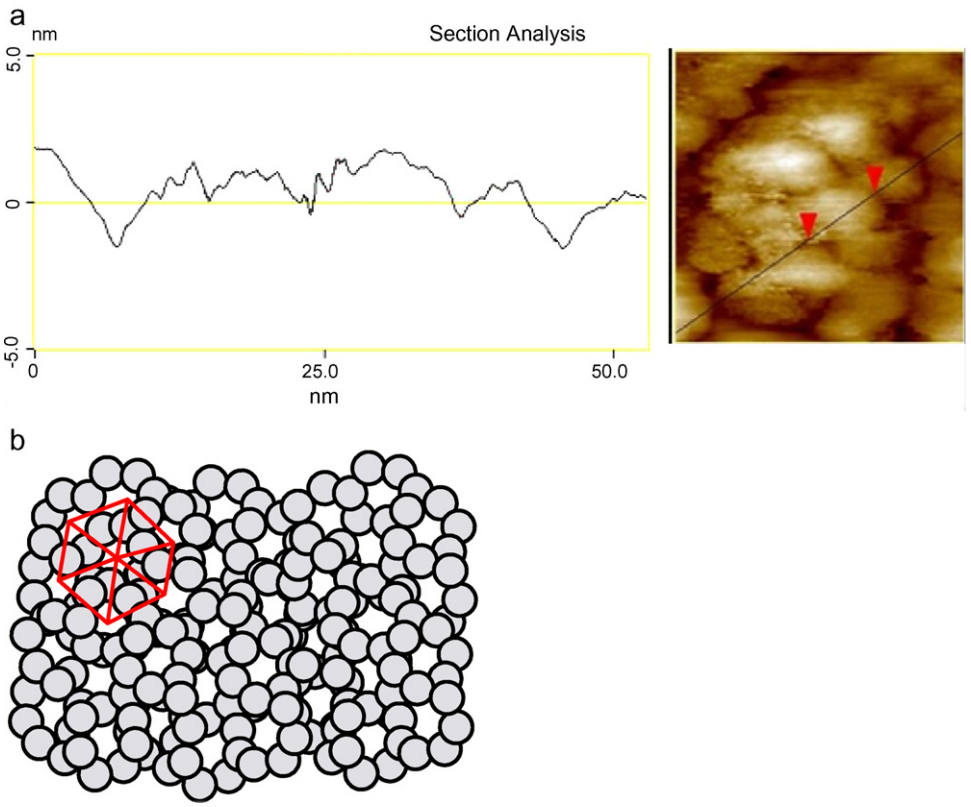

Fig. 4. (a) STM image of Pt mesoporous thin film (50 × 50 × 10 nm). Left: Section analysis of the catalyst surface; (b) schematic view of the sectional cut of the catalyst layer, showing the hexagonal pore array (red line) and the interpore walls formed by nanospheres like those shown in (a). (For interpretation of the references to color in this figure legend, the reader is referred to the web version of the article.)

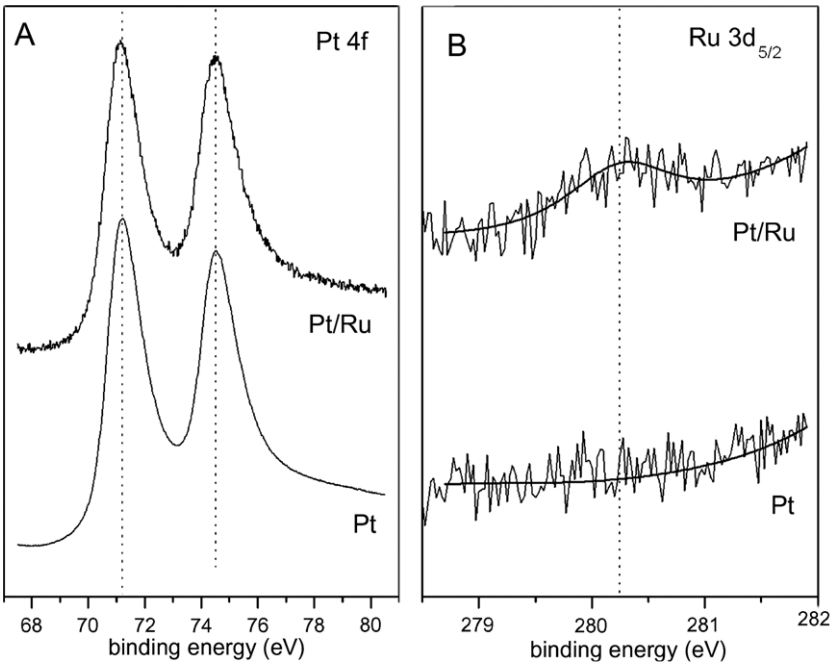

Fig. 5. (a) Pt 4f and (b) Ru $3d_{5/2}$ XP spectra of the mesoporus Pt and Pt/Ru alloy thin films.

mately 9 nm, which is a size comparable to that expected for the thickness of the interpore wall. A schematic representation of the sectional cut of the catalyst layer, which scale with the obtained pore and particle sizes is observed in Fig. 4b. In this 2D representation the red line indicates the hexagonal pore structure, and it can be seen that the interpore walls are formed by particles of size similar to the pore diameter. This structure is consistent with the FESEM micrographs shown in Fig. 2e and f.

The surface compositions of mesoporous Pt and Pt/Ru alloy thin films were determined by XPS. Fig. 5a shows the Pt 4f XP spectra of mesoporous Pt and Pt/Ru alloy catalysts. In both cases we observe the expected doublet with binding energies of 71.2 eV (Pt $4f_{7/2}$) and 74.5 eV (Pt $4f_{5/2}$) which is indicative of metallic Pt. Fig. 5b shows the corresponding Ru $3d_{5/2}$ XP spectra of mesoporous Pt and Pt/Ru alloy catalysts. Clearly, in the case of the pure Pt film there is no signal present in the Ru $3d_{5/2}$ region of the spectra as expected, whereas in the case of the Pt/Ru alloy there is a small peak present at 280.2 eV binding energy. The surface composition estimated from the integrated Pt 4f and Ru $3d_{5/2}$ XP intensities yields a value of 97% Pt and 3% Ru which is in excellent agreement with the compositions estimated by EDX. The fact that the compositions estimated by EDX and XPS are very similar indicates that there is no Ru segregation from or away the surface, resulting in a catalyst with homogeneous composition.

3.2. Electrochemical characterization

3.2.1. H_2 adsorption–desorption

The catalysts exhibit well-defined H_2 adsorption/desorption peaks in the potential region −205 to 245 mV (vs. Ag/AgCl (sat)), after 10 cycles between −205 and 645 mV (vs. Ag/AgCl (sat)) at 100 mV s^{-1}.

The electrochemical active surface area of the catalysts was estimated using the integrated charge in the H_2 adsorption/desorption region. For alloys with low ruthenium content, this method is considered a good approach [39].

The electrodeposited masses determined by direct weight ranged from 0.115 mg cm^{-2} to 0.250 mg cm^{-2}, depending on the electrodeposition overpotential. Faradaic efficiencies of around 43–45% were observed at low overpotentials, but decays at higher overpotentials and become very low at very high overpotentials (lower than −450 mV). This could be due to both, diffusional control originated by the high viscosity of the mixture, and the presence of other reducible species.

The EAS for the Pt and Pt/Ru catalysts along with their masses and the Faradaic efficiencies are reported in Table 1. The EAS for the Pt catalyst prepared at −300 mV is smaller than for that prepared at −400 mV and −500 mV, as expected considering that, as mentioned above, at high electrodeposition overpotentials the formed structures have larger particles are formed [23]. The Pt/Ru alloys exhibit essentially the same behavior, as observed in Table 1 and Fig. 2b and d.

3.2.2. Methanol oxidation

Area normalized current densities (j) and mass activity (i) for methanol oxidation on Pt and Pt/Ru catalysts can be observed in the CV of Fig. 6a. The onset potential for methanol oxidation is around 445 mV (vs. Ag/AgCl(sat)) on the Pt catalysts, and around 100 mV lower for the Pt(97)/Ru(03) alloy, that are a typical values for these catalysts [20,40]. The electrocatalytic activities for methanol oxidation are summarized in Table 1 only for the Pt obtained at −400 mV and the Pt/Ru obtained at −425 mV (vs. Ag/AgCl(sat)), the conditions where the electrodepositions have shown well defined nucleation/growth curves.

The chronoamperometry response of the mesoporous Pt and Pt/Ru alloy is shown in Fig. 6b. In the case of Pt, the rapid current decrease at short times could be attributed to the poisoning of the catalyst surface [41]. The rate of current decay becomes exponen-

Table 1
Electrodeposition potential, electrochemical active surface area (EAS), electrodeposited mass, Faradaic efficiencies (FE) and area-normalized current density of the catalysts (j).

Catalyst	Potential [mV]	EAS [$m^2\ g^{-1}$]	Mass [mg cm^{-2}]	FE	j [mA cm^{-2}]
Pt	−300	25.1	0.117	45%	
Pt	−400	40.7	0.128	43%	0.0062
Pt/Ru	−400	40.1	0.243	45%	
Pt/Ru	−425	47.1	0.116	35%	0.0159

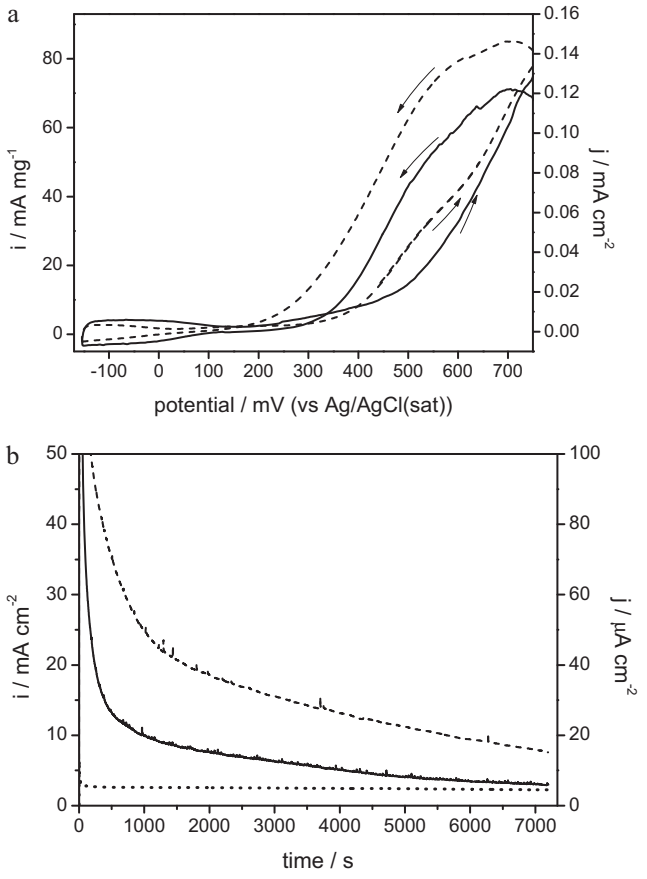

Fig. 6. (a) Cyclic voltammogram of Pt (continuous line) and Pt(97)/Ru(03) alloy (dashed line) in 1 M CH_3OH and 0.5 M H_2SO_4; (b) chronoamperometry of methanol oxidation of Pt (continuous line) and Pt(97)/Ru(03) alloy (dashed line) and commercial Pt/C (dotted line) in 1 M CH_3OH and 0.5 M H_2SO_4 obtained at 445 mV vs. Ag/AgCl (sat).

tial at longer time and a limit mass activity of 2.42 A g^{-1} is reached considering the geometrical area of the electrode, which is approximately 5% higher than the obtained for the E-TEK Pt/C (E-TEK) catalyst (2.29 A g^{-1}). For the Pt/Ru alloy, a mass activity of 7.52 A g^{-1} was achieved under the same conditions.

Thus, it is observed that a small amount of Ru in the composition of the catalyst enhances its catalytic activity, as well as, that the ruthenium is not segregated of the platinum. This assertion was confirmed by the GI-XRD results, which show a shift towards smaller cell parameters for the Pt/Ru metallic phases, in agreement to the previous literature results [42–44].

The alloying degree was calculated following the technique described by Antolini et al. [42,43] based on the comparison of the lattice parameters of the Pt/Ru and the Pt catalysts. An alloying degree of 40.3% was obtained for the Pt(97)Ru(03), which can be considered as a high degree of alloying [44]. In addition, the XRD peaks are broader for the bimetallic sample (FWHM values are of 1.2° and 1.9° for Pt and Pt(97)Ru(3), respectively). Although the GI-XRD experiment does not permit a quantitative analysis of the grain size, we concluded that the walls of the Pt/Ru sample are composed of smaller nanoparticles.

Recently, Takai et al. [20] prepared a Pt(96)Ru(04) alloy having hexagonal 2D structure with a interpore distance of 6 nm, using a dual-templating method with Brij 56® as mesostructural template and porous anodic alumina membranes as morphological template. The obtained catalyst exhibits an EAS of 20 m^2 g^{-1} and a mass activity of 2.5 A m g^{-1} (reached at 30 min in 1 M CH_3OH at 60 °C). In contrast, our Pt(97)/Ru(03) catalyst has, at 25 °C, a higher EAS (47 m^2 g^{-1}), and a higher mass activity for methanol oxidation (7.5 A g^{-1}) than those reported by Takai et al. [20], and they would be even higher if the comparison were carried out at the same temperature [45].

Moreover, the transient time used by Takai et al. [20], was 30 min, which is not enough to reach the stationary state, so the differences in mass activity between both catalysts would be even larger. Thus, the measured mass activity of our Pt and Pt(97)Ru(3) catalysts at t = 30 min are 7.9 A g^{-1} and 19.3 A g^{-1}, respectively, much higher than the reported for the stationary state, Guo et al. [41] prepared nanoparticulated Pt/Ru catalysts in different atomic ratios and the chronamperometric analysis shows that, for the catalysts with lower ruthenium ratio, Pt(80)Ru(20), a mass activity of 15 A g^{-1} at room temperature, at 400 mV (vs SCE) and at t = 2000 s. Under these conditions, our catalyst with a much lower Ru content, has a mass activity of 18.5 A g^{-1}, The EAS for a material with small pore diameter, like that prepared by Takai et al. [20], is expected to be larger than for a catalyst with large pore size electrodeposited using F127®, contrary to the experimentally observed. This unexpected behavior can be explained considering that our catalyst, with a similar mesoporous hexagonal structure, has larger methanol accessibility due to its large pore diameter, which permits an enhanced mobility of the reactants to the active sites. On the other hand, the observed onset potential for methanol oxidation is similar for both catalysts.

4. Conclusions

In the present work, mesoporous Pt and Pt(97)Ru(03) with large pore Hexagonal 2D structures were successfully synthesized using a F127® template, on a gold support. The large electrochemical surface area observed for Pt and Pt/Ru catalysts prepared at high overpotentials can be accounted for the irregular structure formed when growth dominates over nucleation.

The onset potential for methanol oxidation is approximately 100 mV lower for the Pt(97)Ru(03) alloy as compared to the Pt catalyst, while the limit current density of the Pt/Ru alloy is more than twice the value for Pt. Compared to a Pt(96)Ru(04) alloy obtained with a liquid crystal template, our catalyst exhibits a smaller electroactive area but a higher current density for methanol oxidation, probably due to a better methanol accessibility as a consequence of the pore size and pore connectivity.

In summary, the procedure described in this work for preparation of mesoporous Pt/Ru catalyst by electrodeposition, using F127® block copolymer as template, can provide a method for the generation of high-performance anodes for DMFC.

Acknowledgements

The authors thank financial support from Agencia Nacional de Promoción Científica y Tecnológica (PICT Start Up 35403, PICT 34518), and CONICET (PIP 5977). The contribution of National Synchrotron Light Laboratory (LNLS, Campinas, Brazil) is gratefully acknowledged. HRC, FJW, GAP and GSI are permanent research fellows of CONICET. EAF thank to CONICET for a graduate fellowship.

References

[1] J. Jiang, A.J. Kucernak, Electroanal. Chem. 543 (2003) 187–199.
[2] G.S. Attard, P.N. Bartlett, N.R.B. Coleman, J.M. Elliott, J.R. Owen, J.H. Wang, Science 278 (1997) 838–840.
[3] X. Cui, J. Shi, L. Zhang, M. Ruan, J. Gao, Carbon 47 (2009) 186–194.
[4] H. Kim, P. Kim, J.B. Joo, W. Kim, I.K. Song, J. Yi, J. Power Sources 157 (2006) 196–200.
[5] A. Kucernak, J. Jiang, Chem. Eng. J. 93 (2003) 81–90.
[6] G.S. Attard, S.A.A. Leclerc, S. Maniguet, A.E. Russell, I. Nandhakumar, P.N. Bartlett, Chem. Mater. 13 (2001) 1444–1446.

[7] J.M. Elliott, G.S. Attard, P.N. Bartlett, N.R.B. Coleman, D.A.S. Marcel, J.R. Owen, Chem. Mater. 11 (1999) 3602–3609.
[8] G.S. Attard, C.G. Goltner, Patent PCT/GB1998/000587, WO 1998/037997 (1998).
[9] G.S. Attard, P.N. Bartlett, N.R.B. Coleman, J.M. Elliott, J.R. Owen, Langmuir 14 (1998) 7340–7342.
[10] G.A. Planes, G. García, E. Pastor, Electrochem. Commun. 9 (2007) 839–843.
[11] P. Alexandridis, T.A. Hatton, Colloid Surf. A 96 (1995) 1–46.
[12] G. Wanka, H. Hoffmann, W. Ulbricht, Macromolecules 27 (1994) 4145–4159.
[13] D.Y. Zhao, J.L. Feng, Q.S. Huo, N. Melosh, G.H. Fredrickson, B.F. Chmelka, G.D. Stucky, Science 279 (1998) 548–552.
[14] D.Y. Zhao, Q.S. Huo, J.L. Feng, B.F. Chmelka, G.D. Stucky, J. Am. Chem. Soc. 120 (1998) 6024–6036.
[15] D.Y. Zhao, J.Y. Sun, Q.Z. Li, G.D. Stucky, Chem. Mater. 12 (2000) 275–279.
[16] F.Q. Zhang, Y. Yan, H.F. Yang, Y. Meng, C.Z. Yu, B. Tu, D.Y. Zhao, J. Phys. Chem. B 109 (2005) 8723–8732.
[17] C.Z. Yu, J. Fan, B.Z. Tian, D.Y. Zhao, G.D. Stucky, Adv. Mater. 14 (2002) 1742–1745.
[18] L. Huang, H. Wang, Z. Wang, A. Mitra, D. Zhao, Y. Yan, Chem. Mater. 14 (2002) 876–880.
[19] P. Van der Voort, M. Benjelloun, E.F. Vansant, J. Phys. Chem. B 106 (2002) 9027–9032.
[20] A. Takai, T. Saida, W. Sugimoto, L. Wang, Y. Yamauchi, K. Kuroda, Chem. Mater. 21 (2009) 3414–3423.
[21] J. Jiang, A. Kucernak, Chem. Mater. 16 (2004) 1362–1367.
[22] T.L. Knutson, M.L. Bollinger, W.H. Smyrl, J. Electrochem. Soc. 155 (2008) F17–F21.
[23] W. Lizcano-Valbuena, V.A. Paganin, C.A.P. Leite, F. Galembeck, E.R. Gonzalez, Electrochim. Acta 48 (2003) 3869–3878.
[24] M.L. Lin, C.C. Huang, M.Y. Lo, C.Y. Mou, J. Phys. Chem. C 112 (2008) 867–873.
[25] J.W. Guo, T.S. Zhao, J. Prabhuram, R. Chen, C.W. Wong, Electrochim. Acta 51 (2005) 754–763.
[26] A. Lewera, W.P. Zhou, C. Vericat, J.H. Chung, R. Haasch, A. Wieckowski, P.S. Bagus, Electrochim. Acta 51 (2006) 3950–3956.
[27] M.M.E. Duarte, A.S. Pilla, J.M. Sieben, C.E. Mayer, Electrochem. Commun. 8 (2006) 159–164.
[28] Y.L. Kawamura, T. Sakka, Y.H. Ogata, J. Electrochem. Soc. 152 (2005) C701–C705.
[29] M.R. Khelladi, L. Mentar, A. Azizi, A. Sahari, A. Kahoul, Mater. Chem. Phys. 115 (2009) 385–390.
[30] Y. Lai, F. Liu, J. Li, Z. Zhang, Y. Liu, J. Electroanal. Chem. 639 (2010) 187–192.
[31] M. Klotz, P.A. Albouy, A. Ayral, C. Ménager, D. Grosso, A. Van der Lee, V. Cabuil, F. Babonneau, C. Guizard, Chem. Mater. 12 (2000) 1721–1735.
[32] G.J. Soler-Illia, E.L. Crepaldi, D. Grosso, D. Durand, C. Sanchez, Chem. Commun. (2002) 2298–2299.
[33] E.L. Crepaldi, G.J.A.A. Soler-Illia, D. Grosso, F. Ribot, F. Cagnol, C. Sanchez, J. Am. Chem. Soc. 125 (2003) 9770–9786.
[34] R. Ivanova, P. Alexandridis, B. Lindmann, Colloid Surf. A 185 (2001) 41–53.
[35] S. Qi, Z.G. Wang, Polymer 19 (1998) 4639–4648.
[36] M. Clerc, A.M. Levelut, J.F. Sadoc, J. Phys. II France (1991) 1263–1276.
[37] G.J.A.A. Soler-Illia, E.L. Crepaldi, D. Grosso, C. Sanchez, Curr. Opin. Colloid Interface Sci. 8 (2003) 109–126.
[38] M. Etienne, A. Quach, D. Grosso, L. Nicole, C. Sanchez, A. Walcarius, Chem. Mater. 19 (2007) 844–856.
[39] S. Trasatti, A. Petrii, Pure Appl. Chem. 63 (1991) 711–734.
[40] D.H. Lim, W.D. Lee, D.H. Choi, D.R. Park, H.I. Lee, J. Power Sources 185 (2008) 159–165.
[41] J.W. Guo, T.S. Zhao, J. Prabhuram, R. Chen, C.M. Wong, Electrochim. Acta 51 (2005) 754–763.
[42] E. Antolini, F. Cardellini, J. Alloys Compd. 315 (2001) 118–122.
[43] E. Antolini, L. Giorgi, F. Cardellini, E. Passalacqua, J. Solid State Electrochem. 5 (2001) 131–140.
[44] L. Ma, C. Liu, J. Liao, T. Lu, W. Xing, J. Zhang, Electrochim. Acta 54 (2009) 7274–7279.
[45] J.L. Cohen, D.J. Volpe, H.D. Abruña, Phys. Chem. Chem. Phys. 9 (2007) 49–77.